As originally published in the SMTA Proceedings.

Microalloying Effects of Sb and Ag on the Microstructural Evolution of Eutectic Sn-Bi Alloys

Hannah Fowler, Sukshitha Achar Puttur Lakshminarayana, Sui Xiong Tay, Yifan Wu, Ganesh Subbarayan, John Blendell, Carol Handwerker
Purdue University
Indiana, USA
fowlerh@purdue.edu

ABSTRACT

The low melting temperature of eutectic Sn-Bi alloys (139°C) makes eutectic Sn-Bi a suitable low-temperature alternative to high-Sn, lead-free solders in electronics packaging. The low eutectic temperature allows for a peak reflow temperature of 180°C rather than the 240°C reflow temperature required for Sn-Ag-Cu (SAC) alloys. Lower reflow temperatures reduce warpage-induced solder joint defects. However, the strain-rate sensitivity of Sn-Bi alloys results in poor drop-shock performance despite having high reliability in thermal cycling. As reported in the literature, microalloying with Sb and Ag has shown improved ductility and lower strain-rate sensitivity that are known to enhance drop-shock performance and result in a more reliable joint. In this paper, we will compare the bulk microstructure of eutectic Sn-Bi with Sb and Ag additions to solder joints on Cu substrates and ENIG (electroless nickel immersion gold) surface finishes. Our results demonstrate how small changes in composition from the substrate or surface finish alter the microstructure in this system and the impact that heterogenous microstructures can have on the mechanical properties of Sn-Bi solder joints.

Key words: eutectic Sn-Bi, low-temperature, solder, lead-free

INTRODUCTION

Using low temperature, Sn-Bi solders (LTS) reduces heat-induced warpage during reflow and the manufacturing defects caused by warpage by allowing for lower peak reflow temperatures. Figure 1 illustrates head-on-pillow, open circuits, and bridging defects caused by the package warpage at higher reflow temperatures.[1]

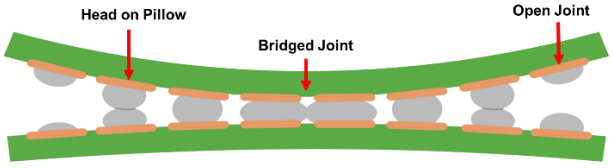

Figure 1. Representation of the heating-induced warpage that occurs at higher reflow temperatures. This warpage can be prevented by using low-temperature solders (reflow <200°C).[1]

Tin-silver-copper alloys, with 1-4wt% Ag and 0.5wt% Cu, require a peak reflow temperature of 240°C while Sn-Bi-based LTS alloys can be reflowed below 200°C. Although using Sn-Bi LTS alloys reduces the number of warpage defects during reflow, Sn-Bi alloys are highly strain-rate dependent. The literature shows definitively that Sn-Bi LTS alloys perform well at the low strain-rates during thermal cycling but is highly alloy dependent at the high strain rates seen in drop-shock reliability tests. However, since many of the alloys are proprietary, their compositions are not known. Fundamental studies of the effect of known alloying additions of mechanical and thermomechanical performance of these alloys may be useful in alloy design to increase ductility, reduce strain-rate sensitivity, and improve creep resistance leading to higher drop-shock reliability and their use in a wider range of applications.

The literature has shown that small alloying additions of Sb, Ag, and Cu may provide the improvements required for better drop-shock reliability. Silver additions are known to refine the Sn-Bi eutectic microstructure formed during solidification and reduce coarsening and to increase shear strength and creep resistance of Sn-Bi solders which improves thermal cycling reliability.[2] Silver-based Ag_3Sn intermetallic (IMC) particles may be present in the liquid due to the low solubility of Ag in Sn-Bi liquid and these particles are prone to coarsening during reflow and aging. According to thermodynamic calculations, silver additions must be limited to less than or equal to 0.7 wt% to ensure that most of the Ag_3Sn dissolves during reflow at 180°C. Although Sakuyama et al.[3] have suggested that large Ag_3Sn particles may have an embrittling effect[3] no such effect has been observed for Ag additions of 1wt%. Additions of Cu and Sb have also been shown to limit coarsening of the Sn-Bi eutectic.[4] However, increasing the Sb concentration increases the melting temperature of the alloy and allows large SnSb IMC particles to form during solidification. It has been reported that large SnSb IMC particles enable both transgranular and intergranular cracks to propagate.[3–5] One strategy is to limit Sb additions to below the amount where large SnSb IMCs form. This, in turn, allows for the formation of small, sub-micron SnSb particles that form on Sn/Bi interfaces during cooling with some Sb remaining in solid solution. The combination of Ag and Sb provides solid solution strengthening (Sb) and precipitation hardening (Sb, Ag) in Sn-Bi.[3,4] Fine Ag_3Sn and SnSb particles at Sn-Bi interfaces may pin dislocations and inhibit grain boundary migration. Solid solution Sb may change creep kinetics, inhibit dislocation motion, and segregate to grain boundaries which can also inhibit grain boundary migration. In terms of co-doping, additions of Ag and Sb have been observed to prevent grain coarsening.

The behavior of Sn-Bi alloys is unusual. For metals in general, an increase in strengthening leads to a loss of ductility. In contrast, additions of Sb to Sn-Bi alloys have been shown to increase Sn-Bi ductility significantly without decreasing strength.[3] An open question is how that is possible.

The optimal compositions of Sn-Bi alloys with Ag and Sb additions have not been established, and the mechanisms behind the increase in ductility from Sb addition while maintaining alloy strength are not understood. Precipitation hardening by pinning of dislocations by precipitates and solid solution strengthening typically reduce ductility, but the Sn-Bi-Sb system shows high ductility. Some studies suggest that the primary role of the fine SnSb IMC particles along the Sn-Bi boundary is to prevent Bi from coarsening and limit grain growth.[3,6] It is our contention that this is not enough, i.e., that superplastic flow and grain size refinement during deformation may be occurring, producing the observed high ductility, while maintaining strength. The first stage in developing this understanding is characterizing microstructure development as a function of alloy composition, particularly with respect to Sb and Ag additions, as well as other elements (Cu, Au, and Ni) that are introduced into the alloys by reactions with the organic solderability preservative (OSP) - Cu and ENIG (Au, Ni). The second stage is determining the solubility limits of Sb and Ag additions to eutectic Sn-Bi solders and other elements in multi-component alloys. In parallel, understanding the mechanisms by which Sb and Ag increase both strength and ductility will be essential to alloy design. This paper is a preliminary report on the quantification of microstructures and solubility limits in multi-component systems, from Sn-Bi on OSP Cu (three components) to Sn-Bi-Ag-Sb alloys on ENIG (six components.) In particular, we (1) identify the room temperature solubility limit of Sb in Sn and the composition ranges where large SnSb do not form, (2) describe the complex microstructures associated with solidification and then cooling below the eutectic temperature, and (3) present plans for additional microstructure quantification studies in conjunction with mechanical property measurements.

EXPERIMENTAL DESIGN

Six near eutectic, Sb- and Ag-containing Sn-Bi solder alloys were obtained in the form of 500 µm spheres from Scientific Alloys Corporation. The compositions of the custom alloys were confirmed with ICP-MS to be within an acceptable range of the requested Bi-42Sn-*x*Sb-*y*Ag (*x*= 0.5, 1, 2 and *y* = 0 or 1) with +/-2 wt% Sn, +/-0.1 wt% Sb, and +/- 0.3 wt% Ag. The compositions from the ICP-MS results can be seen in Table 1. In general, the alloys are more Sn-rich than expected, the Ag compositions are above and below 1wt% (with a range 0.7-1.1 wt%), but the Sb additions are as requested.

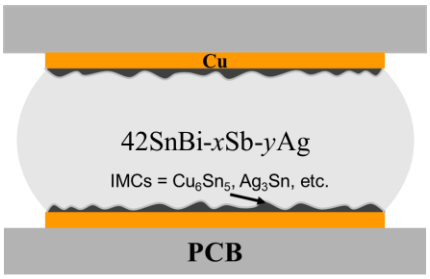

Figure 2. A schematic of a typical solder joint showing the location and composition of the IMC layer.

The solder spheres were fluxed and placed on FR4 BGA test boards with either an OSP or an ENIG surface finish and reflowed in a 3-zone tabletop reflow oven with a peak reflow temperature of 180°C. After reflow, the resulting solder joints range from quaternary to senary (six-component) alloys due to the dissolution of Cu from the Cu/OSP substrate or the dissolution of Ni and Au from the ENIG substrate. A representation of one of these solder joints can be seen in Figure 2. The bulk solder alloys were also studied to better understand what microstructure effects were specifically related to the Sb and Ag additions versus the Cu, Au, Ni additions from the surface finishes. The solder spheres were reflowed on a non-wetting substrate under the same conditions as the solder joints to maintain consistent reflow profiles and cooling rates.

Table 1. Expected solder sphere compositions of Bi-42Sn-*x*Sb-*y*Ag (*x* = 0.5, 1, 2 and *y* = 0 or 1) versus the measured results from ICP-MS.

42SnBi-*x*Sb-*y*Ag Alloys		Sn	Bi	Sb	Ag
0.5Sb	Expected	42	57.5	0.5	0
	Measured	43.1	56.5	0.4	0
1Sb	Expected	42	57	1	0
	Measured	43.3	55.7	1.0	0
2Sb	Expected	42	56	2	0
	Measured	43.7	54.3	2.0	0
0.5Sb-1Ag	Expected	42	56.5	0.5	1
	Measured	44.5	53.9	0.6	1.1
1Sb-1Ag	Expected	42	56	1	1
	Measured	42.7	55.5	1.0	0.7
2Sb-1Ag	Expected	42	55	2	1
	Measured	42.2	55.1	1.9	0.7

Electron probe microanalysis (EPMA) - wavelength dispersive spectroscopy (WDS) was used to determine the distribution of Cu, Ag, and Sb IMCs in the different solder alloys. The elements Sn and Sb have significant x-ray peak overlaps, and WDS provides greater spectral resolution than electron dispersive spectroscopy (EDS) to resolve these peaks. Scanning electron microscopy (SEM) in the backscattered electron mode (BSE) is used to identify Sn and Bi, as well as (Au,Ni)Sn_4 particles dispersed in the matrix. The IMC Ag_3Sn particles can be easily identified from height differences of the phases in polished cross-sections, due to the higher hardness of Ag_3Sn than all other phases in the

microstructures. Therefore, a combination of EPMA and SEM images were used for microstructure analysis.

In future testing, nanoindentation will be used to determine the creep behavior and strain-rate sensitivity of eutectic SnBi. The samples for nanoindentation were prepared in the same way as the samples for microstructural analysis, including being mounted in epoxy, cross-sectioned, and polished. Nanoindentation was performed with a Berkovich indenter tip so that the results could be easily compared to previous SnBi nanoindentation experiments in the literature.

RESULTS AND DISCUSSION

Microstructure Analysis

The microstructures seen in the Bi-42Sn-*x*Sb-*y*Ag alloys are highly heterogeneous and include several different intermetallic compounds from reactions between Sn and the alloying elements and different locations in the microstructure. One of these heterogeneous microstructures (Sn-56Bi-1Sb-1Ag on OSP) is shown in Figure 3. This microstructure is representative of the complex microstructures found in all the Sb-containing alloys. All the alloys have Sn dendrites, a SnBi two-phase eutectic lamellar structure that forms between the dendrites, and Bi precipitation in the Sn dendrites and in the Sn in the eutectic during cooling to room temperature. Alloys with 1 wt% Ag addition have Ag_3Sn IMC particles through the solder and at a higher concentration at the solder/substrate interface owing to the Ag_3Sn IMC not completely dissolving at the reflow temperature. At 180°C the solubility of Ag in Sn is 0.8 wt%. With a 180°C peak reflow temperature, 0.2 wt% Ag will be undissolved leaving Ag_3Sn particles in the molten liquid solder.[7]

The resulting microstructure of Sn-55Bi-1Sb-1Ag on OSP shown in Figure 3 contains Sn dendrites, Sn-Bi eutectic, Bi precipitation in Sn dendrites and the Sn phase in the eutectic, Ag_3Sn particles, Cu_6Sn_5 particles, SnSb particles with Bi precipitation inside the particles, and a Cu_6Sn_5 IMC layer at the solder/Cu interface.

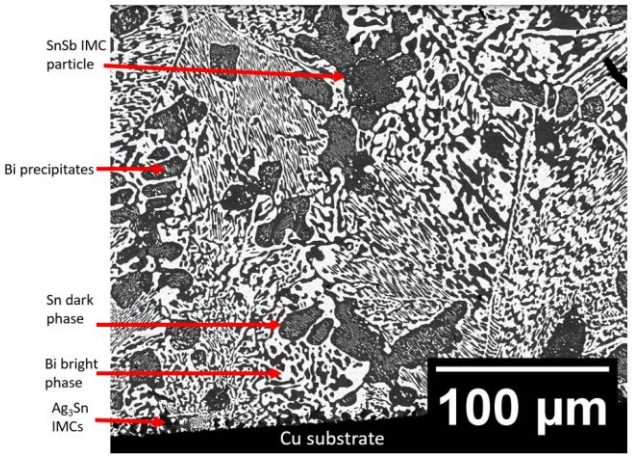

Figure 3. Microstructure of 42Sn-Bi-1Sb-1Ag solder joint on OSP (Cu) in BSE-SEM. The dark phase is Sn, and the bright phase is Bi-rich. IMCs are indicated by arrows.

Depending on the composition, alloys with Sb can have large SnSb particles that form during solidification and SnSb particles that precipitate in Sn during cooling in the solid state to room temperature as the Sb comes out of solution. One of these large SnSb particles is shown in Figure 4 as well as the associated EDS maps. Binary SnSb IMCs are highly non-stoichiometric with a range of stability that changes as a function of temperature. This results in precipitation of Sn inside or on the surfaces of SnSb particles during cooling. In addition, there is substantial solubility of Bi in SnSb which changes as a function of temperature, leading to precipitation of Bi in the SnSb IMC during cooling from the eutectic to room temperature.

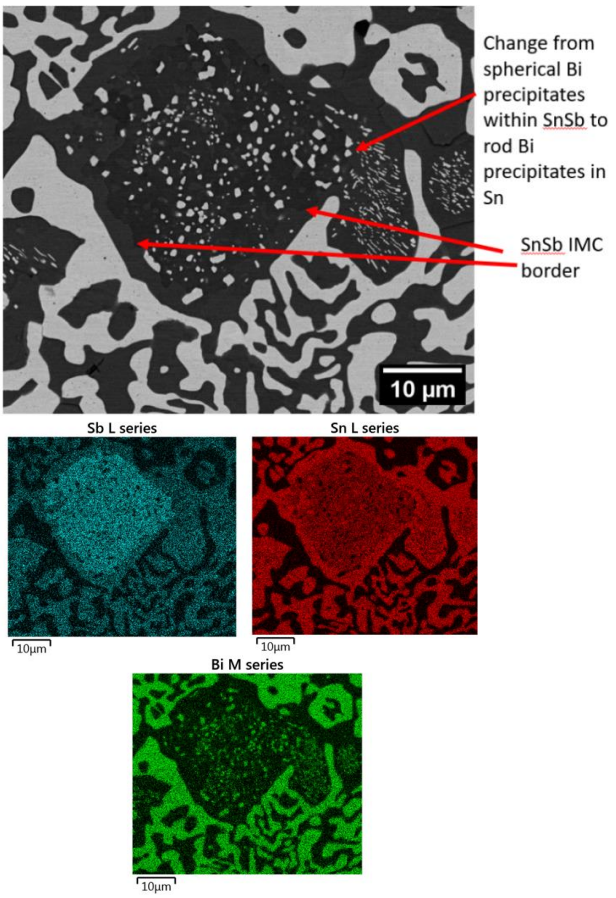

Figure 4. SEM-BSE of a large SnSb IMC particle from a Sn-56Bi-2Sb sample on OSP and the associated EDS maps.

Samples on boards with an OSP surface finish will have Cu dissolution into the system. At 180°C the solubility of Cu in Sn is 0.03 wt%, and a Cu_6Sn_5 IMC layer forms at the solder-Cu interface during reflow. During cooling, the dissolved Cu comes out of solution as Cu_6Sn_5 particles in the molten solder as the solder solidifies.[7] Therefore, widely dispersed Cu_6Sn_5 IMC particles are seen throughout the solder. Samples on boards with an ENIG surface finish will have both Au and Ni dissolution into the solder. The solubility of Au in Sn is 0.14 wt% at 180°C, however, Ni solubility is extremely limited at <0.01 wt% Ni.[7] A Ni_3Sn_4 interfacial IMC layer forms at the solder/ENIG interface during reflow. Upon solidification, $(Au,Ni)Sn_4$ IMC particles form in the bulk solder.

Phase diagram assessments provide insight into the possible evolution of microstructures during solidification and aging, and this is important since these microstructures determine the mechanical behavior of the resulting solder joints. For ternary and higher order alloys, analyzing phase diagrams and solidification paths provide researchers with guidelines for microstructure development that occurs during solidification and cooling to room temperature for different alloy compositions. Phase diagram calculations and solidification modeling are commonly performed using Thermo-Calc, however the available databases are not always the most accurate thermodynamic bases for the phase diagrams being calculated.[8] The Thermo-Calc Sn-Bi phase diagram using the current database, TCSLD4: Solder Alloys v4.0, shows that the eutectic composition for Sn-Bi is 54 wt% Bi, and the models for the Sn-Bi-Sb ternary phase diagrams and any solidification modeling are based on this eutectic composition. However, numerous experimental studies have indicated that the eutectic composition is Sn-58Bi.[9] In the following, an analysis is presented of the microstructures expected using Thermo-Calc and NIST assessments for both the Sn-Bi eutectic composition and the solubility of Sb in near eutectic Sn-Bi alloys.

Figure 5 shows a comparison of the liquidus projections of the Sn-Bi-Sb phase diagram from Thermo-Calc using the database TCSLD4: Solder Alloys v4.0 (54 wt% Bi eutectic) and the NIST solder database (58 wt% Bi eutectic). The liquidus projection shows the primary phase field for each of the elements in the ternary Sn-Bi-Sb system near the eutectic composition. The compositions of the Sn-Bi-Sb alloys in this study are indicated. The Thermo-Calc calculations indicate that two of the three alloys are in the Bi primary phase field. This means that Bi precipitates would form first during solidification. The NIST estimate indicates that the alloy with the lowest Sb concentration is in the Sn primary phase field. This means all the Sn-rich alloys in the study (Table 1) will have primary Sn that forms as Sn dendrites.

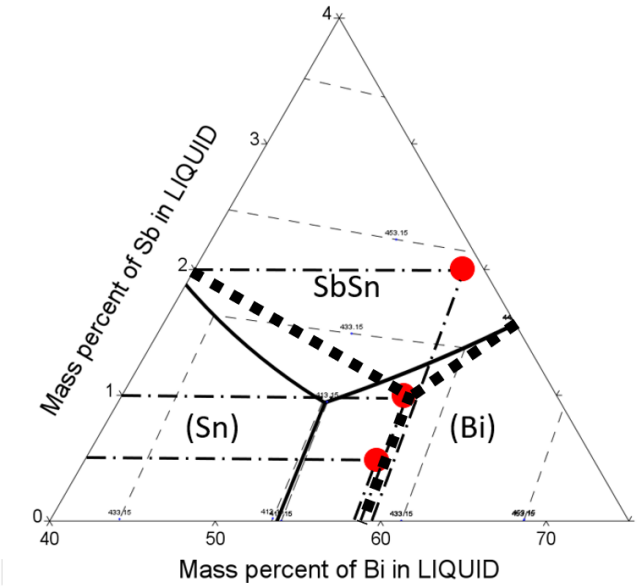

Figure 5. Sn-Bi-Sb liquidus projection modeled in Thermo-Calc using the database TCSLD4: Solder Alloys v4.0.[8] The black solid lines represent the primary phase field boundaries calculated from the Thermo-Calc database that produces a Sn-Bi eutectic composition of 54 wt% Bi. The dotted lines represent potential boundaries based on the NIST Sn-Bi eutectic of 58 wt% Bi. (Note that because of the different scaling of the Sb and Bi axes the slopes of the phase boundary lines are different than when the entire phase diagram is shown with axes from 0 – 100%.)

The matrix of microstructures in Figure 6 shows Sn dendrites in all the alloy compositions as is expected from solidification path analysis of the slightly Sn-rich compositions determined with ICP-MS. The microstructures of all Sb-containing alloys are heterogeneous with multiple morphologies of Sn-Bi microstructures existing in the same sample at many different scales, not just dendrites and eutectic. The multiple eutectic morphologies, the changes in
the dendrites (primary and secondary arm spacings and volume fraction), the internal precipitation of Bi in Sn and of Bi in SbSn at different size scales, and the many intermetallic particles, i.e., Ag_3Sn, Cu_6Sn_5 , SbSn, $(Au,Ni)Sn_4$ at different size scales and locations relative to other phases have made the quantitative microstructure analysis of these alloys challenging.

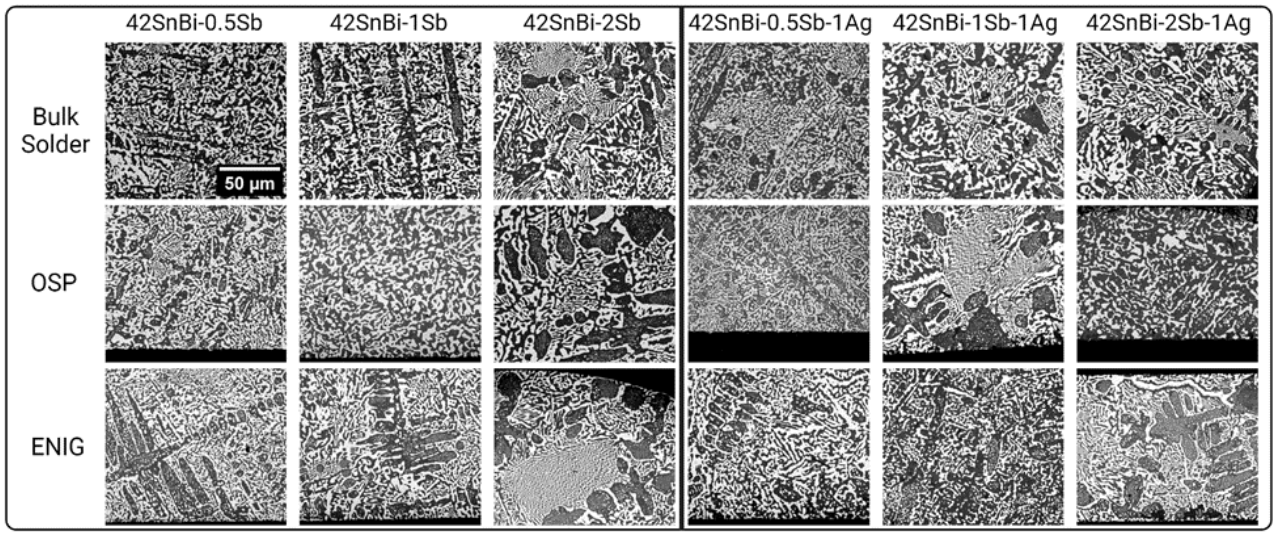

Figure 6. Matrix of SEM-BSE images showing the heterogeneous microstructures found in Bi-42Sn-XSb-YAg alloys. Samples reflowed on OSP have Cu additions and samples reflowed on ENIG have Ni and Au additions.

Composition maps from EPMA-WDS in Figure 7 show fine SnSb IMC particles in Sn along the Sn/Bi interface in all samples containing 1 wt% Sb or 2 wt% Sb. However, no SnSb IMC particles were found in any of the 0.5 wt% Sb samples. This suggests that Sb is soluble in Sn at room temperature at 0.5 wt% Sb. Large SnSb particles were observed at the 2 wt%Sb samples, indicating that this composition solidifies in the SnSb primary phase as indicated in the ternary liquidus projection in Figure 5, followed by Sn dendrite formation before the formation of the eutectic. As previously observed, 1 wt% Ag is above the solubility limit at 180 °C and large Ag_3Sn IMC particles are in higher concentration at the solder/substrate interface in both OSP and ENIG samples. Particles of Ag_3Sn away from the solder/substrate interface are finer, indicating their precipitation from the liquid during solidification. The locations that Ag_3Sn and SnSb IMC particles form do not appear to be correlated in any way. Particles of Cu_6Sn_5 are

found throughout the bulk resulting from Cu dissolution into the solder from OSP surface finishes. At the copper-solder interface, Cu_6Sn_5 forms a continuous IMC layer. However, there appears to be a zone near the interface that is denuded of Cu_6Sn_5 particles relative to the bulk. This denuded zone suggests that any Cu_6Sn_5 that could have formed in the solder near the interface during solidification precipitated on the pre-existing interfacial Cu_6Sn_5 layer.

In ENIG samples, there is a continuous Ni_3Sn_4 IMC layer at the solder/ENIG interface. Sheet-like $(Au,Ni)Sn_4$ IMC particles are found throughout the solder. In addition, a discontinuous $(Au,Ni)Sn_4$ IMC layer is observed between the Ni_3Sn_4 IMC layer and the solder.

If Sb is still soluble in Sn at 0.5 wt% Sb at room temperature, then Sb can provide solid solution strengthening in all three Sb-containing alloys. However, at 0.5 wt% Sb there are not any particles to pin dislocations or grain boundaries to prevent grain growth. Instead of particle pinning, it is possible for there to be Sb solute segregation at the Sn/Bi interfaces within the Sn-rich phase. The segregation of Sb at the Sn/Bi phase boundary could prevent microstructure coarsening and increase ductility of the alloy analogous to how Zn solute segregation at the Bi/Sn interface prevented microstructure coarsening in previous Sn-Bi studies.[10–12] Segregation of Sb at the Bi/Sn phase boundaries would also explain why SnSb precipitates are seen at these boundaries within the Sn phase at higher Sb concentrations.

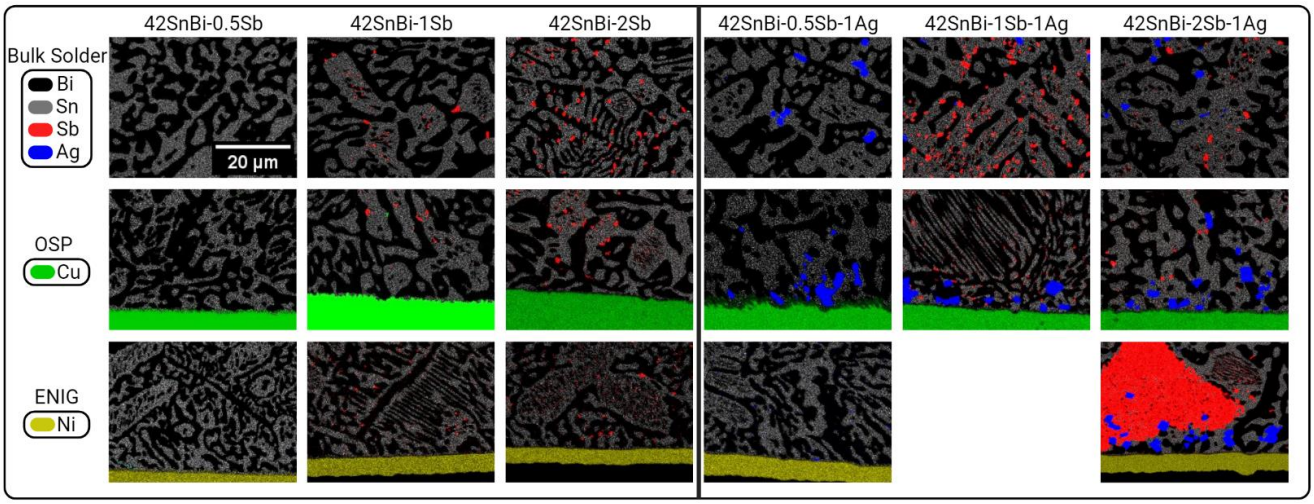

Figure 7. SnSb and Ag_3Sn particle distribution in Bi-42Sn-*x*Sb-*y*Ag alloys shown with EPMA-WDS elemental maps.

The benefits of Sb additions are likely a result of the sub-micron SnSb precipitates and the Sb remaining in solid solution. The large SnSb IMC particles seen in 2 wt% Sb addition are not believed to be beneficial to the mechanical properties of eutectic Sn-Bi and may negatively impact the ductility of the alloy as suggested by previous studies from Sakuyama, et al, Lee et al, and Chen, et al.[3–5] Fine Ag_3Sn precipitates increase alloy strength and creep resistance, but these precipitates can coarsen and lead to a more brittle joint if greater than 1 wt% Ag is added.[3]

CONCLUSIONS AND FUTURE WORK

Small Sb additions to eutectic Sn-Bi solder alloys increase ductility without decreasing alloy strength. Determining the mechanisms behind these beneficial mechanical attributes is important for better alloy development and to understand how to optimize these alloys for better drop-shock reliability. The first step in determining mechanisms is the quantitative characterization of how the microstructure changes with alloy composition. The presence of Sn dendrites in these alloys and the lack of SnSb IMC particles in the 0.5 wt% Sb alloys suggest the NIST Sn-Bi phase diagram is an accurate representation of the Sn-Bi system. If Sb is still soluble in

SnBi at 0.5 wt%, this means that the increase in ductility of SnBi must be primarily caused by solute-related effects such as solid solution strengthening or solute segregation to the phase boundaries rather than by precipitation hardening or precipitate effects. Exactly how these solutes increase the ductility still must be determined from deeper microstructure investigation including interrupted shear testing. Adding Sb at concentrations above 0.5 wt% results in SnSb precipitates, but the solid solution effects are still present. As Sb addition increases, the SnSb precipitates increase in size and increase in quantity. As previously stated, Sakuyama suggested that these larger SnSb particles are the reason why the ductility of SnBi decreased above 5 wt% Sb addition.[3] Preventing these larger SnSb particles from forming seems to be critical for maintaining improved ductility from Sb addition to eutectic SnBi.

The next step in quantification will be to determine the volume fraction of Sn dendrites relative to eutectic and the spatial distribution of the SbSn IMC particles. To obtain the needed statistics, both will require analyzing substantially more solder joints and cross sections than done up to this point. These will be accompanied by nanoindentation testing to study the impacts of Sb and Ag addition on the strain-rate sensitivity and creep resistance of eutectic Sn-Bi alloys and may reveal information on the effects of microstructural heterogeneity. In addition, interrupted monotonic shear testing and fatigue testing will be used to study the microstructural evolution of these alloys after different amounts of deformation. These tests will also show the effects of Sb and Ag alloying on the ductility and strength of these alloys as a solder joint.

ACKNOWLEDGEMENTS

This work was supported in part by Semiconductor Research Corporation (SRC). We gratefully acknowledge helpful discussions with Yaohui Fan and David Bahr of Purdue. The EPMA-WDS images were obtained with the assistance of Will Nachlas at University of Wisconsin-Madison. This work was supported in part by the Research Instrumentation Center in the Department of Chemistry at Purdue University to perform ICP-MS.

REFERENCES

1. Mokler, S., Aspandiar, R., Byrd, K., Chen, O., & Walwadkar, S. (2016). The application of Bi-based solders for low temperature reflow to reduce cost while improving SMT yields in client computing systems. In *Proceeding of SMTA International*.

2. Wang, F., Chen, H., Huang, Y., Liu, L., & Zhang, Z. (2019). Recent progress on the development of Sn–Bi based low-temperature Pb-free solders. In *Journal of Materials Science: Materials in Electronics* (Vol. 30, Issue 4, pp. 3222–3243). Springer New York LLC. https://doi.org/10.1007/s10854-019-00701-w

3. Sakuyama, S., Akamatsu, T., Uenishi, K., & Sato, T. (2009). Effects of a Third Element on Microstructure and Mechanical Properties of Eutectic Sn-Bi Solder. *Transactions of The Japan Institute of Electronics Packaging*, *2*(1), 98–103. https://doi.org/10.5104/jiepeng.2.98

4. Lee, H. T., Lin, H. S., Lee, C. S., & Chen, P. W. (2005). Reliability of Sn-Ag-Sb lead-free solder joints. *Materials Science and Engineering A*, *407*(1–2), 36–44. https://doi.org/10.1016/j.msea.2005.07.049

5. Chen, B. L., & Li, G. Y. (2004). Influence of Sb on IMC growth in Sn–Ag–Cu–Sb Pb-free solder joints in reflow process. *Thin Solid Films*, *462–463*(SPEC. ISS.), 395–401. https://doi.org/10.1016/J.TSF.2004.05.063

6. Li, J. G., Ma, X., Zhou, M. B., Ning, X., & Zhang, X. P. (2018). Effects of Sb addition on the microstructure and mechanical performance of Sn58Bi based alloys and the solder joints. *Proceedings - 2018 19th International Conference on Electronic Packaging Technology, ICEPT 2018*, 457–461. https://doi.org/10.1109/ICEPT.2018.8480722

7. Fan, Y., Wu, Y., Dale, T. F., Lakshminarayana, S. A. P., Greene, C. v., Badwe, N. U., Aspandiar, R. F., Blendell, J. E., Subbarayan, G., & Handwerker, C. A. (2021). Influence of Pad Surface Finish on the Microstructure Evolution and Intermetallic Compound Growth in Homogeneous Sn-Bi and Sn-Bi-Ag Solder Interconnects. *Journal of Electronic Materials*, *50*(12), 6615–6628. https://doi.org/10.1007/S11664-021-09256-1/FIGURES/16

8. Andersson, J. O., Helander, T., Hoglund, L., Shi, P. F., & Sundman, B. (2002). Thermo-Calc 2021a, TCSLD4: Solder Alloys v4.0, Computational tools for materials science. *Calphad*, *26*, 273–312.

9. Lee, B.-J., Oh, C.-S., & Shim, J.-H. (1996). Thermodynamic Assessments of the Sn-ln and Sn-Bi Binary Systems. *Journal of Electronic Materials*, *25*(6).

10. Hirata, Y., Yang, C. han, Lin, S. kang, & Nishikawa, H. (2021). Improvements in mechanical properties of Sn–Bi alloys with addition of Zn and In. *Materials Science and Engineering: A*, *813*, 141131. https://doi.org/10.1016/J.MSEA.2021.141131

11. Zhou, S., Mokhtari, O., Rafique, M. G., Shunmugasamy, V. C., Mansoor, B., & Nishikawa, H. (2018). Improvement in the mechanical properties of eutectic Sn58Bi alloy by 0.5 and 1 wt% Zn addition before and after thermal aging. *Journal of Alloys and Compounds*, *765*, 1243–1252. https://doi.org/10.1016/J.JALLCOM.2018.06.121

12. Zhou, S., Shen, Y. A., Uresti, T., Shunmugasamy, V. C., Mansoor, B., & Nishikawa, H. (2019). Improved mechanical properties induced by In and In & Zn double additions to eutectic Sn58Bi alloy. *Journal of Materials Science: Materials in Electronics*, *30*(8), 7423–7434. https://doi.org/10.1007/S10854-019-01056-Y/TABLES/4